# TIME-STEPPING FINITE-ELEMENT ANALYSIS OF DYNAMIC ECCENTRICITY FAULT IN A THREE-PHASE SALIENT POLE SYNCHRONOUS GENERATOR

## J. Faiz and M. Babaei

Science and Research Branch
Islamic Azad University
Tehran, Iran

## J. Nazarzadeh

Shahed University
Tehran, Iran

## B. M. Ebrahimi

Center of Excellence on Applied Electromagnetic Systems
School of Electrical and Computer Engineering
University of Tehran
Tehran, Iran

## S. Amini

Niroo Research Institute
Tehran, Iran

**Abstract**—In this paper, two-dimensional time-stepping finite-element (TSFE) method is performed for modeling and analyzing of a salient pole synchronous generator with different degree of dynamic eccentricity (DE) fault. TSFE analysis is used to describe the influence of DE fault on the flux distribution within the generator and no-load voltage profiles at low and high field current is obtained for healthy and faulty cases. Comparing the magnetic flux distribution of healthy and faulty generators helps to detect the influence of DE fault. Also, it can be seen at no-load condition with low excitation current, the effect of the eccentricity is considerable compared to that of the rated excitation current. Since the calculation of inductances of the machine is the most

---

Corresponding author: M. Babaei (mba_babaei@yahoo.com).

important step for fault analysis and diagnosis, the self- and mutual-inductances of the stator phases and rotor windings are calculated in the eccentric generator. Double periodic phenomenon is observed in inductances profile of stator phases due to the DE fault. Finally, spectrum analysis of stator current of two generators with different design parameters is used to diagnosis the significant harmonics in the presence of DE fault.

## 1. INTRODUCTION

The bulk of electrical power is presently generated by means of synchronous generators. Abnormal conditions may occur during regular operation of the generators due to the stress involved in the electromechanical energy conversion process. Abnormal conditions lead the generators to permanent damage that commonly called fault. Mechanical faults are one of the major faults in electrical machines caused by mechanical parts in bearing, shaft and coupling [1–4]. It can be resulted in serious damage to the stator and rotor windings and cores, unless detected at an early stage. Eccentricity fault is considered as a mechanical fault in which, the conformity of the symmetrical axis of rotor and stator is lost and air gap becomes non-uniform. Shaft deflection, inaccurate positioning of the rotor with respect to the stator, worn bearing, stator core movement, bent rotor shaft, oval stator core, misalignment of bearing and mechanical resonance at critical speed are reasons for the eccentricity faults [5–9]. The static, dynamic and mixed eccentricities are the three-types of this fault that have been recognized. In the case of static eccentricity (SE) fault, rotation axis is adopt on rotor symmetry axis and stator axis displaced with respect to them. Consequently, the minimum radial air gap length is fixed and time-independent. In the DE fault, stator axis coincides with rotation axis and the rotor symmetry axis is displaced to the two axes. Cross-section of the generator in the healthy and DE faults is shown in Figure 1. $O_s$ and $O_r$ are the centerlines of the stator and rotor, respectively. Finally, in mixed eccentricity (ME) fault, all of the above mentioned axes are displaced with respect to each other. The rotor eccentricity is one of the prominent causes of magnetic asymmetries and induced shaft voltages. Use of shaft signal is an alternative approach to diagnose and detect DE fault in synchronous generator [10, 11]. With use of a resistor-capacitor integrator, the shaft flux-linkage signal is extract from the shaft voltage signal. It is shown that there are exist some frequencies in the shaft flux-linkage signal related to the DE fault. Stator current signature analysis is a common approach for detection of asymmetrical
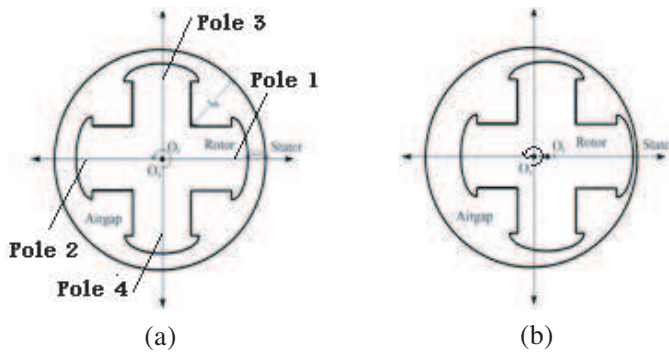
**Figure 1.** Cross-section of a salient pole synchronous generator: (a) healthy, and (b) with DE fault.

conditions in electrical machine. It is used for DE fault diagnosis in round-rotor synchronous generator [7, 9]. Simulation and experimental results show that the 17th and 19th harmonic of the line current of the round rotor synchronous generator increased with increase of the DE degree. Therefore, the 17th and 19th harmonics can be used as a convenient index for the dynamic eccentricity fault diagnosis in a round-rotor synchronous generator. Winding function method (WFM) is an analytical approach that frequently used for modeling and an analyzing the electrical machine under faults conditions. This method has been used to model of a salient pole synchronous machine under dynamic eccentricity fault [1, 7, 9]. However, since magnetic saturation and slots effects on magneto-motiveforce (MMF) have been ignored in this method, the results of it are not accurate.

TSFEM is a precise numerical method applied in time dependent problem. Some features such as electric circuit coupling and moving band technique, make this desirable approach for electrical machines modeling and analysis. It is capable to takes into account the real geometry of generator, nonlinear properties of ferromagnetic materials, spatial distribution of stator winding, type of rotor and stator slots shape around the air gap and different asymmetrical conditions in generator [12, 13].

Eccentricity fault in induction motors is widely investigated [14–20], but a very few papers deals with such faults in synchronous generators. Hence, study of the generator performance under this fault seems to be necessary.

Modeling and analysis of DE fault in salient pole synchronous generator using TSFEM has not been investigated yet. In this paper, a typical salient pole synchronous generator is simulated in

healthy and DE faulty condition using a two-dimensional TSFEM. For this, FE formulations are presented and the model of the generator is constructed using the real specifications, geometry parameters, material properties, and physical layout of the windings. Flux distribution and generator self- and mutual-inductance profiles of stator phases and rotor winding are presented in healthy and different DE degrees. No-load voltage profile of the faulty generator is also obtained and generator current signature analysis is presented in the subsequent section to detect harmonic related to the DE fault.

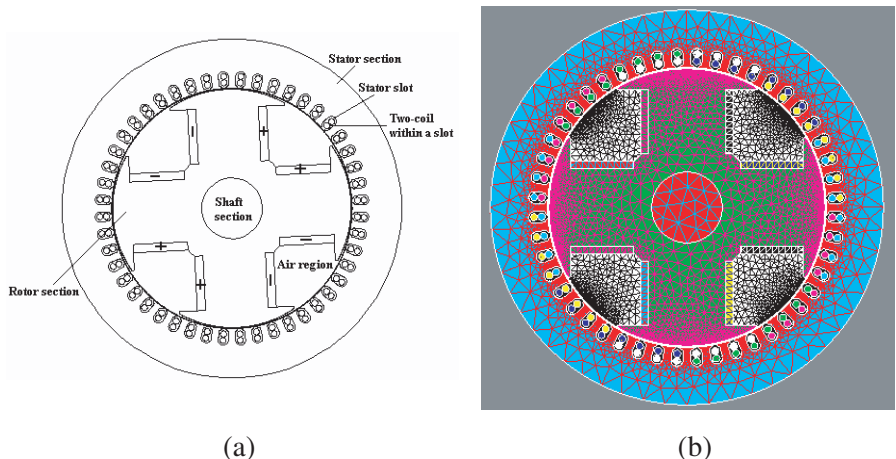## 2. FE MODELING OF SALIENT-POLE SYNCHRONOUS GENERATOR

An appropriate geometrical CAD model and mathematical model are required for performance prediction of the salient pole synchronous generator in healthy and faulty conditions using FEM. This generator is heterogeneous, with non-linear magnetization stator and rotor cores. A three-phase, 4-poles synchronous generator with rated parameters of 50 KVA, 400 V (line to line voltage) and 0.8 lag is candidate to perform FE modeling and analysis. Details of the generator dimensions, windings and materials are given in Table 1. The three-phase fractional pitch windings distribution of the generator is also shown in Figure 2. The rotor excitation winding is a concentrated one and distributed over the pole body.

**Table 1.** Synchronous generator specifications for FE modeling.

| Parameter | Value | Parameter | Value |
|---|---|---|---|
| Min. air gap length | 1.4 mm | Rotor shoe width | 144 mm |
| Max. air gap length | 2.7 mm | Rotor pole height | 23.1 mm |
| Stack length | 202 mm | Rotor shoe height | 3 mm |
| No. of stator slots | 48 | Shaft diameter | 76 mm |
| Stator slot pitch | 19.6 mm | Stator material | ST12 |
| Stator inner diameter | 300 mm | Rotor material | CK45 |
| Stator outer diameter | 423 mm | Shaft material | 1814 |
| No. of rotor poles | 4 | No. of rotor win. turn | 117 |
| Rotor poles width | 78 mm | turns in each phase | 24 |
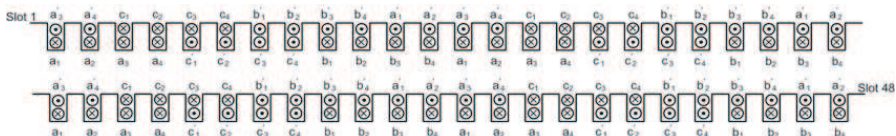
**Figure 2.** Fractional pitch distribution of stator three-phase windings for a four-pole salient-pole synchronous generator.



(a)                                    (b)

**Figure 3.** (a) Cross-section of salient-pole synchronous generator model for FE analysis, and (b) finite elements mesh.

## 2.1. Geometrical Modeling of Salient Pole Synchronous Generator

Geometrical structure of the salient pole synchronous generator should be implemented into the FE package in this stage. From the basic geometry, nonlinear properties of the magnetic materials and winding layout of the typical generator, the FE approach is implemented. A model of the healthy salient pole synchronous generator cross-section created into the FEM is shown in Figure 3(a). It is performed using Flux2D FE software package.

In the moving electromagnetic systems, it is necessary to introduce the speed in the equations. The equation which covers this section is as follows:

$$\nabla \times \left( \frac{1}{\mu} \nabla \times \vec{A} \right) + \sigma \left( \frac{\partial \vec{A}}{\partial t} - \vec{v} \times \left( \nabla \times \vec{A} \right) \right) = \vec{J} \tag{1}$$

where $J_0$ is the current density in $z$-axis direction, $\sigma$ is the electrical
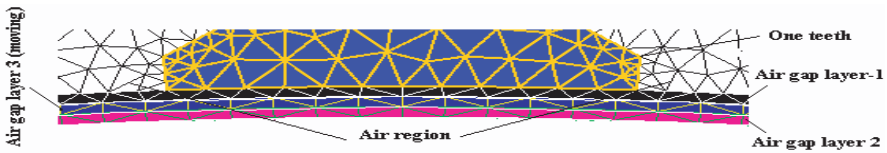
**Figure 4.** FE meshes around air gap region.

conductivity, $v$ is the relative speed and $A$ is the magnetic vector potential. Using a reference frame which is assumed constant under the study part, (1) can be expressed as follows:

$$\nabla \times \left( \frac{1}{\mu} \nabla \times \vec{A} \right) + \sigma \left( \frac{\partial \vec{A}}{\partial t} \right) = \vec{J} \tag{2}$$

In the FE analysis, such reference frame is created by placing a mesh on the surface of the moving part and movement or transformation occur only within the elements that are placed around the moving element [21]. FEM calculations required to generate a correspondent mesh of finite elements. The algorithm of the software application that is used for FEM mesh generation. The mesh must be dense enough for precise calculation and also not consuming a very long computational time. After several attempts for generation the optimal mesh, the most appropriate mesh is obtained. This mesh provides calculation with high precision and at reasonable computational time. In this case, the most convenient mesh type is chosen to be triangular and as presented in Figure 3(b). Also, some details provided in the air-gap region are shown in Figure 4. It is prepare for implementation of the moving band technique and the air-gap splitting into three layers, where the middle one is the moving band. In this technique at every time step only the element in the moving band were re-meshed [22].

## 2.2. Connection of Electrical Circuits to the FE Regions

In modeling of generator, the position of moving parts of generator must be taken into account, because the magnetic forces depend on the position of these moving parts. These positions, in turn, influence the magnetic field within the generator. Therefore, for full and suitable modeling, a link between the fields, circuits, and motion must be established. At this end, only a dc field voltage applied to the terminal of the generator rotor are required as the known input value and voltage and phase current are evaluated as unknown values. Also, transient equations of external circuit showing the electrical supplies and circuit elements must be coupled with the field equations in FEM. Finally,
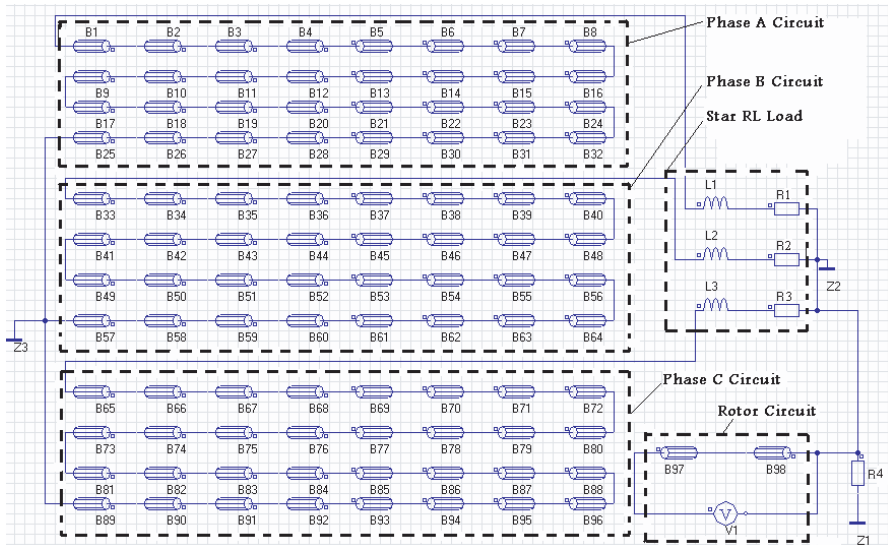
**Figure 5.** Electrical circuit for modeling of the stator phases, rotor winding and RL load to FE implementation.

motion must be combined with the field equations in FEM. The circuit can be coupled to the external load circuit and forms the new circuit equations. A set of coils is connected according to the winding layout and forms the machine circuit with external terminals.

Electrical circuit of stator and rotor is shown in Figure 5, in which each coil of phases and field winding will be linked to the magnetic regions. They represent the conductors in the stator slots and rotor windings. The rated star RL load is taken into account to model the full-load condition of the generator. It is known that:

$$\nabla \times \vec{B} = \frac{\vec{J}}{\nu} \tag{3}$$

$$\vec{B} = \nabla \times \vec{A} \tag{4}$$

where $\nu$ is the reluctivity of the magnetic material. With use of (3) and (4), the governing two-dimensional transient magnetic equation of the field within the generator is as follows:

$$\nabla \times \nu \nabla \times \vec{A} = \vec{J} \tag{5}$$

and the current density obtained as follow:

$$\vec{J} = -\sigma \frac{\partial \vec{A}}{\partial t} - \sigma \frac{\Delta V}{l} \tag{6}$$

where $\Delta V$ is the potential difference along the length of the conductor, $t$ is the time, and $l$ is the conductor length. To link the circuit and field equations, it is necessary to calculate the total current of each conductor. The total current of each conductor is obtained by integration of (6) over the cross section of the conductor. The current is as follows:

$$i = \iint \sigma \left( \frac{\partial A}{\partial t} + \frac{\Delta V}{l} \right) ds \qquad (7)$$

Combination of (5) and (6) leads to:

$$\nabla \times \nu \nabla \times \vec{A} + \sigma \frac{\partial \vec{A}}{\partial t} + \sigma \frac{\Delta V}{l} = 0 \qquad (8)$$

This is used in massive conductors, where the skin effect is calculated. $A$ matrix is used to represent a general circuit which has voltage supply $(E)$, resistance $(R)$, and inductance $(L)$, where

$$[E] = [R][i] + [L]\frac{di}{dt} \qquad (9)$$

Applying the standard method of Galerkin, the general FE matrix equation is obtained:

$$\begin{bmatrix} G & H & 0 \\ 0 & W & D \\ 0 & D^T & -z \end{bmatrix} \begin{bmatrix} A \\ \Delta V \\ i \end{bmatrix} + \begin{bmatrix} Q & 0 & 0 \\ H^T & 0 & 0 \\ 0 & 0 & -L_0 \end{bmatrix} \frac{\partial}{\partial t} \begin{bmatrix} A \\ \Delta V \\ i \end{bmatrix} = \begin{bmatrix} J \\ 0 \\ -xE \end{bmatrix} \qquad (10)$$

where $N$ and $xE$ is the weighting function of Galerkins method and induced voltage, respectively. Also:

$$G_{ij} = \int \nu \nabla N_i \nabla N_j ds \qquad (11)$$

$$H_{ij} = \int_K \sigma N_i ds \qquad (12)$$

$$W_{KK} = \int_K \sigma ds \qquad (13)$$

$$Q_{ij} = \int \sigma N_i N_j ds \qquad (14)$$

$$L_0 = \int J N_i ds \qquad (15)$$

Integrations of $G$, $Q$, and $J$ are carried out over the whole model, whereas for $W$ and $H$ they are over conductor "$K$". $R$ and $L$ are the diagonal matrices of resistances and inductances, respectively. $D$ is the

sparse matrix, where an entry of $+1$ and $-1$ represents the direction of current flow in a conductor. Equation (10) can be conveniently written as

$$MX + K\frac{dX}{dt} = U \tag{16}$$

which can be solved by an appropriate numerical method, where

$$M = \begin{bmatrix} G & H & 0 \\ 0 & W & D \\ 0 & D^T & -z \end{bmatrix}, \quad K = \begin{bmatrix} Q & 0 & 0 \\ H^T & 0 & 0 \\ 0 & 0 & -L_0 \end{bmatrix} \tag{17}$$

$$U = \begin{bmatrix} J \\ 0 \\ -xE \end{bmatrix}, \quad X = \begin{bmatrix} A \\ \Delta V \\ i \end{bmatrix} \tag{18}$$
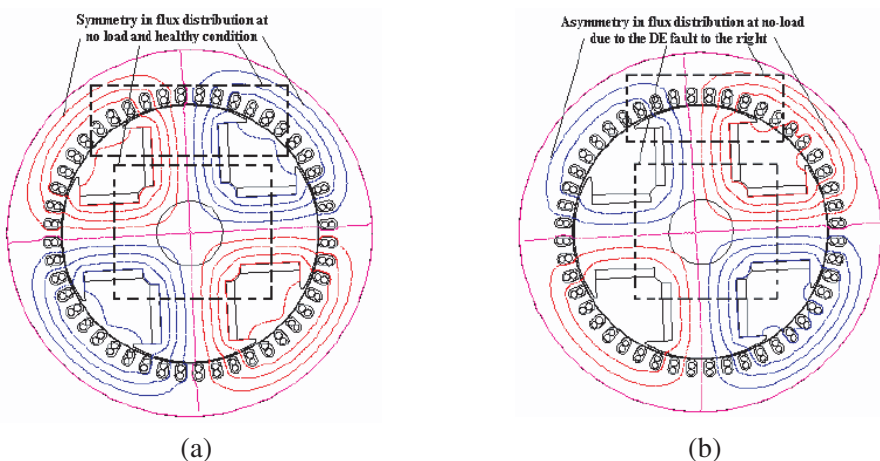
$X$ and consequently magnetic potential vectors $A$ and current $I$, are determined by solving (16).

## 3. FINITE-ELEMENT SIMULATION

The DE degree is defined as follows [23, 24]:

$$DE = \frac{r}{g} \times 100 \tag{19}$$

where $g$ is the radial air gap length in the case of no eccentricity and $r$ is the displacement of the rotor in the horizontal direction.



(a)                        (b)

**Figure 6.** Magnetic flux distribution in generator: (a) healthy, and (b) with 40% SE to the right at no-load and arbitrary rotor position with 2A excitation current.

### 3.1. Impacts of DE on Flux Lines Distribution within Generator

Computation of the field in the salient-pole synchronous generator for healthy and 40% DE generator is started from the system of the Maxwell's equations, which describes the magnetic field in closed and bounded systems. The magnetic field equations are solved in the given structure via the FE approach. Flux distribution within healthy generator and a generator with 40% DE to the right at no-load and arbitrary rotor position with 2A excitation current has been shown in Figure 6, while Figure 7 presents the corresponding flux distribution at rated excitation. It can be seen that the both side of the generator cross-section are identical in the healthy condition and the eccentricity has not clearly affect of the flux distribution within generator at both no load conditions. It is also observed that at the lower excitation current at the no-load, sensitivity of the flux distribution due to the eccentricity is larger compared to the rated excitation current. The reasons are: 1) The air gap of salient pole synchronous generator is inherently large; due to the large gap between the two adjacent poles. Therefore, eccentricity will not clearly affect the total magnetic reluctance of generator magnetic circuit, and therefore the flux distribution within the generator, and 2) the eccentricity is capable to more clearly affect the total reluctance of the generators in low excitation current, in which the generators



(a)                                                        (b)
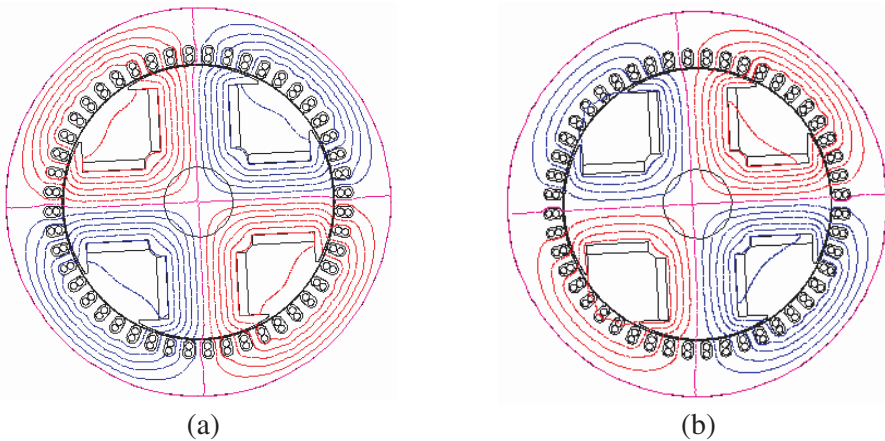
**Figure 7.** Magnetic flux distribution in generator: (a) in healthy, and (b) with 40% SE to right and arbitrary rotor position with 12A excitation current.

magnetic circuit are linear. Therefore, the full reluctance paths of the generators are dominantly determined by the air gap reluctance. In rated excitation, generator saturates intentionally (with 12A dc excitation current). Therefore, the reluctance of the iron core increases significantly and variation of the air gap reluctance does not have a noticeable effect on the total reluctance of the flux lines' paths. So, as seen in Figure 7, eccentricity cannot affect generator flux pattern considerably, when operating at the high excitation current.

## 3.2. Effects of DE Fault on Inductances Profile of Synchronous Generator

Inductance profiles of the windings are the most important characteristics in the modeling and analyzing the synchronous generators. To investigate the performance of the generator under different fault conditions, the inductances of the rotor and stator circuits must be calculated precisely [25, 26].

Due to the symmetrical distribution of the windings in the generators slots, the inductance profile of stator windings will have identical variation with a phase shift in the presence of the eccentricity. Consequently, one phase of stator (phase A) is considered in this paper.
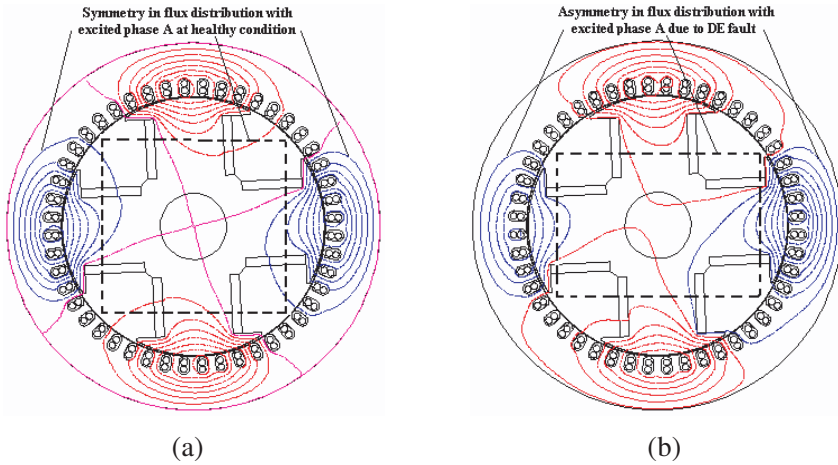
### 3.2.1. Effects on Self-inductance Profiles of Stator Phases

Self inductance of phase A is calculated from the flux-linkage ($\lambda$) seen by the phase when 12A dc current is passed through it, with other windings currents is zero as follows:

$$L_{aa} = \frac{\lambda_{aa}}{I_a} \Big|_{i_b, i_c, i_f = 0} \tag{20}$$

Flux distribution with phase A excited under healthy and with 40% DE have been shown in Figure 8. Symmetrical distribution of flux in the cross-section at healthy condition is clear. Also, asymmetrical flux distribution in the case of 40% DE is noticeable. At 40% DE, the air gap distribution on the rotor pole shoes 1 and 2 (Figure 1) change in opposite direction.

However, there is approximately the same change in the rotor pole shoes 3, 4. Therefore, the rotor poles 3, 4 have the same effect and the rotor poles 1, 2 have the opposite effect on the reluctance path of magnetic flux in the generator cross-section. Consequently, the flux distribution around poles 3, 4 are identical, while it is different for poles 1, 2. Figure 9(a) shows the self-inductance of phase A in the healthy generator and the generator with different DE degrees for different rotor position from 0° to 360° taking rotational steps of 3°. It is clear

**Figure 8.** Magnetic flux distribution within generator with excited phase A: (a) healthy, and (b) with 40% DE to the right.
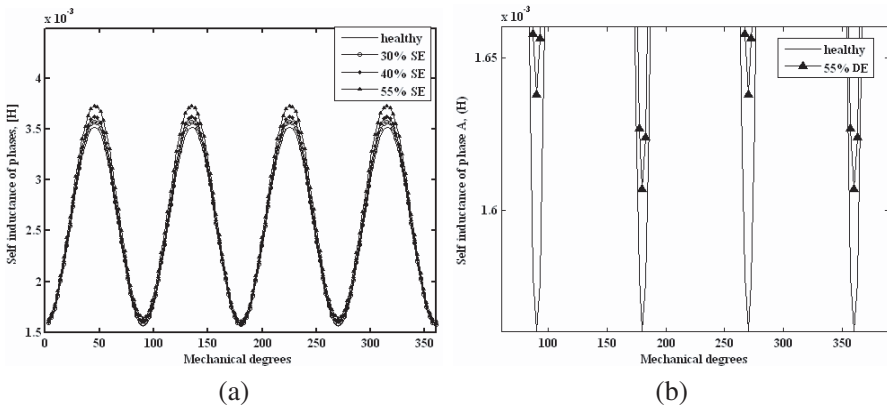


**Figure 9.** (a) Self-inductance profiles of phase A of stator in healthy and eccentric generator, and (b) variation of minimum selfinductance of phase A in healthy generator and generator with 55% DE degree.

that the minimum and maximum amplitude of the self inductance of the phase A rises with the increase of DE. As seen, unequal minima of the inductance profiles occurs in the profile by increase of the DE degree. The minimum variation of the self-inductance of phase A is shown in Figure 9(b). The reason of above mentioned phenomenon is that the phase A seen the minimum self flux twice instead of four times with DE fault; Because of symmetry variation of poles 3, 4

**Table 2.** Comparison of minimum/maximum amplitude of generator inductances for different DE degree in respect to the healthy condition in (%).

| Percent of dynamic eccentricity degree | self inductance of phases | mutual inductance between phases | mutual inductance between phases and the rotor winding | self inductance of the rotor winding |
|---|---|---|---|---|
| **30** | 0.89/1.02 | −3.96/0 | −4.28/4.28 | 9.99 |
| **40** | 1.53/3.03 | −5.28/0 | −7.14/7.14 | 13.32 |
| **55** | 3.01/5.96 | −8.81/0 | −10.57/10.57 | 18.27 |

and asymmetry between poles 1, 2 the half symmetry of generator cross-section instead of four. Variation of the minimum and maximum amplitudes of the self-inductance of phase A at 30%, 40% and 55% DE in respect to the healthy condition given in Table 2.

*3.2.2. Effects on Mutual-inductance Profiles of Stator Phases*

Mutual-inductance between phases (phase A and phase B) is calculated from the flux- linkage seen by the phase B when 12A dc current passes through phase A, with the currents in other winding set to zero as follows:

$$L_{ab} = \frac{\lambda_{bb}}{I_a} \big|_{i_b,i_c,i_f=0} \tag{21}$$

Figure 10(a) shows the mutual-inductance profile between phase A and B in healthy and different DE degrees. Figure 10 and Table 2 indicate that: 1) The maximum amplitude of the mutual healthy inductance of phases A and B are approximately identical for different eccentricity values, 2) the minimum amplitude of the mutual-inductance decreases with increasing DE, 3) the phenomenon occurred in $L_{aa}$ profile, is also exist in $L_{ab}$ profile; because the flux produced by phase B seen by phase A is two times per cycle instead of four due to the previous mentioned reason, and 4) variation in the minimum amplitude of the mutual-inductance in 30%, 40% and 55% DE are larger than that of the self-inductance at the same DE degrees.
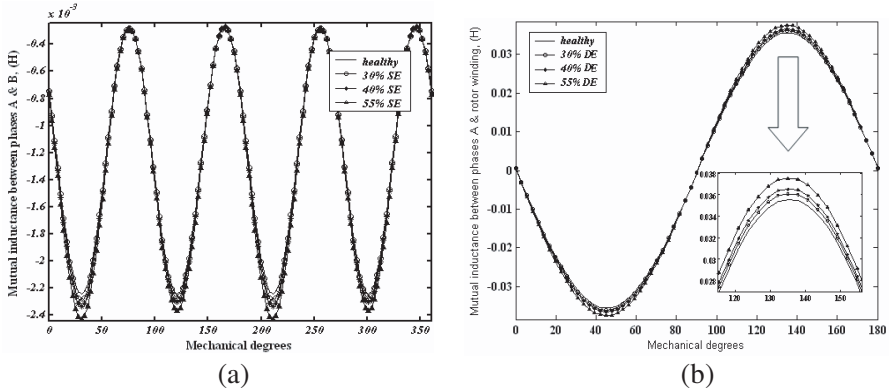
**Figure 10.** (a) Mutual-inductance profiles between stator phase A and B in healthy and eccentric generator, and (b) mutualinductance profiles between the stator phase A and the rotor winding in healthy and eccentric generator.

### 3.2.3. Effects on Mutual-inductance Profiles between Stator Phases and Rotor Winding

The mutual- inductance between stator phase A and the rotor winding is calculated from the flux-linkage seen by the rotor winding with rated current in phase A and the currents in the other windings set at zero as follows:

$$L_{af} = \frac{\lambda_{aa}}{I_f} \mid_{i_a, i_b, i_c = 0} \tag{22}$$

Figure 10(b) shows the mutual-inductance profile between phase A and the rotor winding in healthy and the generator with different DE degrees. As seen in Figure 10(b) and Table 2: 1) The peaks value of the inductance are changing by equal amount, and 2) the phenomenon does not occur in the $L_{af}$ profile with increase in DE degree; because the rotor winding sees the same flux-linkage of phase A of stator over a full revolution of the rotor ($360°$) in different DE degrees.

### 3.2.4. Effects on Self-inductance Profiles of Rotor Winding

Self-inductance of the rotor winding is calculated from the flux-linkage seen by it when the dc current passes through the winding, while the current in all phase windings are zero as follows:

$$L_{ff} = \frac{\lambda_{ff}}{I_f} \mid_{i_a, i_b, i_c = 0} \tag{23}$$
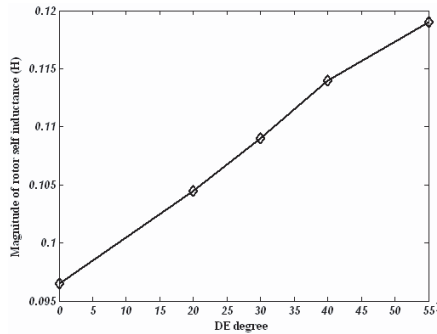
**Figure 11.** Self-inductance profiles of rotor winding in healthy and generator with different DE degree.

The self-inductance of rotor winding is fixed over a full revolution of the rotor. Figure 11 shows the variation in magnitude of the self-inductance of the rotor winding in different DE degrees.

It is observed that the magnitude rises with increase in DE degree and variation of the inductance magnitude is proportional to the DE degree (approximately 3.33% with 10% variation in the DE degree). $L_{ff}$ has the larger variation in the amplitude over different DE degree compared to the $L_{aa}$, $L_{ab}$, and $L_{af}$.

### 3.3. No-load Voltage Profile of Synchronous Generator under DE Fault

No-load voltage profile of phase A of the salient pole synchronous generator is obtained for the healthy generator and for the generator under 20% and 40% DE at the low (2A dc) and rated excitation current (12A dc). Results are presented in Figure 12. All above-mentioned profiles are shown for 180° of the rotor revolution which implies one electrical cycle. As expected in accordance with what mentioned in previous sections, the variations in no-load voltage due to the eccentricity at low excitation current are visibly larger than those of the rated current. For example, 40% DE leads to a 3% increase in the peak voltage amplitude. However, at the rated excitation current, there is no noticeable change in the peak voltage amplitude with the same DE degree. The reason is that at the rated excitation current, generator core is more saturated and the air gap change at the head of pole shoes has no significant influence on the magnetic path and flux density distribution in the air gap. But at 2A dc excitation current, generator behavior is governed by the linear parts of core *B-H* curve
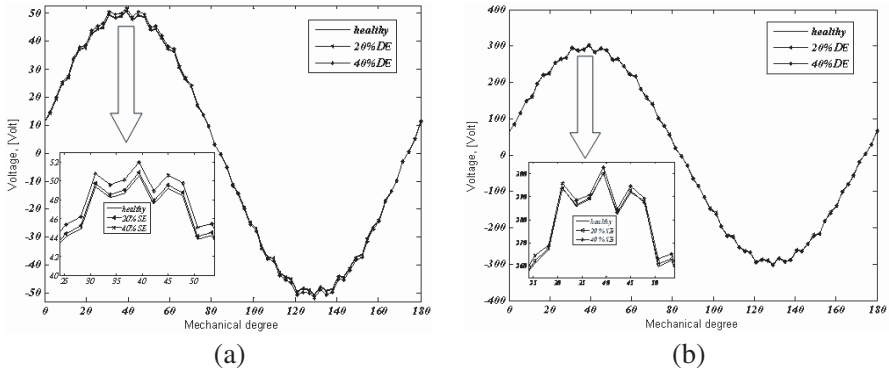
**Figure 12.** No-load voltage profiles of healthy generator and generator with different DE degree, (a) at 2A dc excitation current, and (b) at rated excitation current.

and the air gap change especially at the head of pole shoes can affect the generator flux density in the air gap and consequently the no-load voltage profile.

## 3.4. Spectrum Analysis of the Stator Current at Full-load

The air gap field of the salient pole synchronous generator in normal operation condition contains the fundamental frequency component and some harmonics related to the saturation effect, saliency of the rotor poles, MMF harmonics of stator and rotor. In the presence of DE fault, the harmonics variation of the air gap field is expected due to the asymmetrical air gap distribution. These harmonics can be reflected in the line current of the generator and may be detected from the stator current signature analysis. To analyze the stator current signature, the generator simulated in full-load operating condition using TSFEM and FFT of the current signal have been taken into account. Figure 13(a) shows the frequency spectrum of the stator current for the healthy generator, and Figure 13(b) presents the corresponding curve for the generator with 40% DE degree. The 5th, 7th, 11th, 13th, 17th, 19th, 23rd, and 29th harmonics exist in the line current spectrum even in the healthy condition. Normalized amplitude variation (in dB) of the line current harmonics of a healthy generator and the generator with 10%, 30% and 40% DE degree is shown in Figure 14. This comparison clarifies the importance of taking into account the 29th harmonic. It is observed that the 29th harmonic amplitude increases with rising DE level. No significant increase in the 29th harmonic amplitude occur
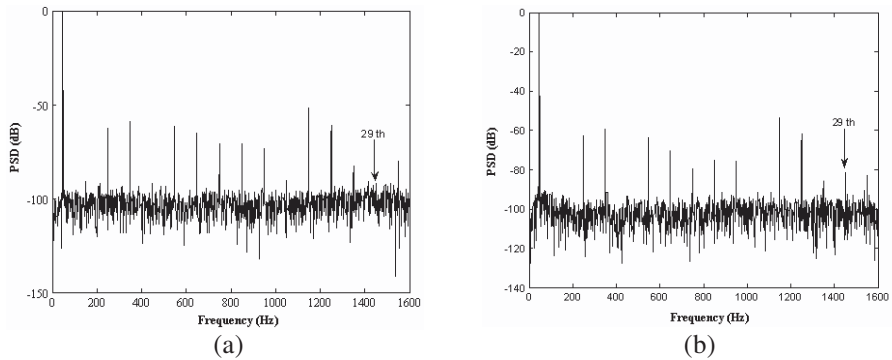
**Figure 13.** Line current spectra of the salient pole synchronous generator, (a) healthy and (b) 50% DE.
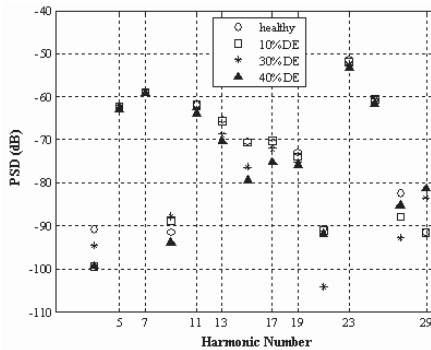


**Figure 14.** Variation of some harmonic amplitude of the line current in healthy generator and the generator with 10%, 30% and 40% DE.

in normal degree of DE (around 10% DE), meanwhile this harmonic increases from $-92\,\mathrm{dB}$ in the healthy generator to $-82\,\mathrm{dB}$ in the generator with 40% DE degree. The 3rd harmonic and its multipliers can be removed from the current spectrum of stator winding with no neutral connection [9]. Also, no pattern exists in the other harmonics (see Figure 14) of stator current with variation of SE degree.

Numerical analysis is also performed on another salient pole synchronous generator with different design parameters and stator current is taking into account. Frequency spectrum of stator line current of healthy generator and generator with 50% DE has been shown in Figure 15. It can be seen that the 19th harmonic is significant and increased about $6\,\mathrm{dB}$ due to the 50% DE. Finally,

another generator with specific parameters design has been selected for test in [1, 7, 27]. Experimental results have been shown that the 17th and 19th harmonics of stator current arise with rise in eccentricity degree and can be utilized as a index for DE fault diagnosis in salient pole synchronous generator. Figure 16 shows the measured frequency spectrum of stator current and importance of taking into account of 17th and 19th harmonics.
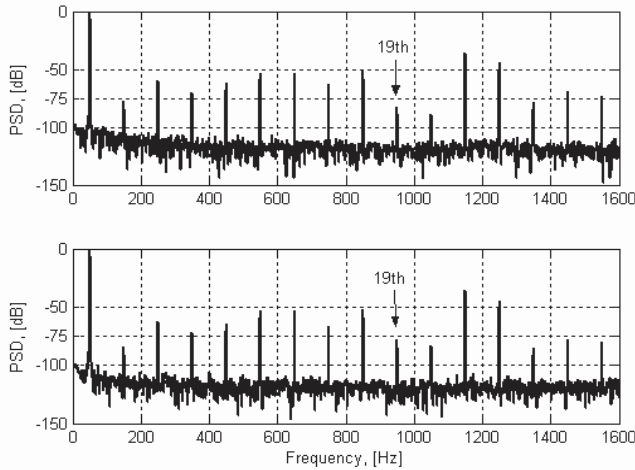


**Figure 15.** Line current spectra of the salient pole synchronous generator with different design parameters, (top) healthy and (bottom) 50% DE.
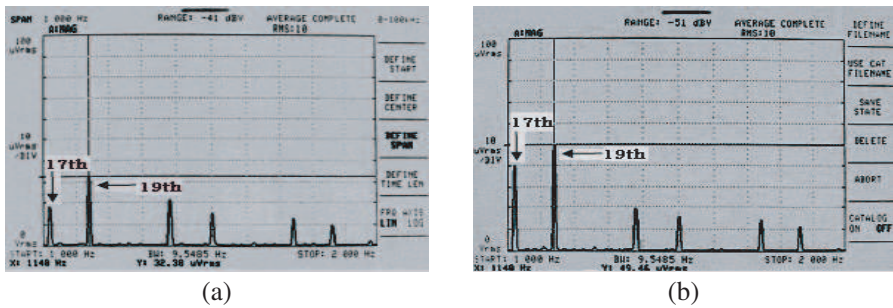


**Figure 16.** Measured frequency spectrum of stator current (1000 Hz–2000 Hz) of a generator with rated frequency of 60 Hz, (a) healthy, and (b) with 50% DE [1, 7, 27].

Therefore, it is concluded from the analysis that the general opinion can not be formulated in eccentricity fault diagnosis for salient-pole synchronous generators with different design parameters.

## 4. CONCLUSION

It was observed from the two-dimensional TSFEM, moderate degree of DE fault has no significant effect on the performance of a salient pole synchronous generator. The effect of DE fault in the generator at no-load with low excitation current is larger than that of high excitation current. This is due to saturation effect of iron core at high excitation current. It also changes inductance profiles of stator phases and rotor winding and this can result in a double periodic phenomenon occur in the self- and mutual-inductance profiles of the stator phases. In addition, variation in the amplitude of the rotor inductances is higher than that of the stator self- and mutual-inductances.

This investigation shows that the effect of eccentricity on the no-load voltage characteristic at rated excitation current is not evident. But at low excitation current, eccentricity can affect the voltage profile. It is found from the stator current spectrum analysis that the some harmonics are significant in the field of DE fault diagnosis of salient pole synchronous generator that dependent to the machine design parameters. Other harmonics may be appearing in the stator current by interaction between the generator parameters with eccentricity fault.

## REFERENCES

1. Al-Nuaim, N. A. and H. A. Toliyat, "A novel method for modeling dynamic air-gap eccentricity in synchronous machines based on modified winding function theory," *IEEE Trans. Energy Conversion*, Vol. 13, No. 2, 156–162, Jun. 1998.
2. Faiz, J., B. M. Ebrahimi, and M. B. B. Sharifian, "Different faults and their diagnosis techniques in three-phase squirrel-cage induction motors — A review," *Electromagnetics Journal*, No. 26, 543–569, 2006.
3. Toliyat, H. A. and S. Nandi, "Condition monitoring and fault diagnosis of electrical machines — A review," *Proc. IEEE-IAS Annu. Meeting*, 197–204, Phoenix, AZ, Oct. 1999.
4. Faiz, J. and I. Tabatabaei, "Extension of winding function theory for nonuniform air gap in electric machinery," *IEEE Trans. Magnetics*, Vol. 38, 3654–3657, 2002.

5.  Faiz, J., I. Tabatabaei, and H. A. Toliyat, "An evaluation of inductances of a squirrel-cage induction motor under mixed eccentric conditions," *IEEE Trans. Energy Conversion*, Vol. 18, 252–258, 2003.

6.  Nandi, S., H. A. Toliyat, and X. Li, "Condition monitoring and fault diagnosis of electrical motors — A review," *IEEE Trans. Energy Conversion*, Vol. 20, No. 4, 719–729, Dec. 2005.

7.  Tabatabaei, I., J. Faiz, H. Lesani, and M. T. Nabavi-Razavi, "Modeling and simulation of a salient-pole synchronous generator with dynamic eccentricity using modified winding function theory," *IEEE Trans. Magnetics*, Vol. 40, No. 3, 1550–1555, 2004.

8.  Tavner, P. J. and J. Penman, *Condition Monitoring of Electrical Machines*, Research Press, Letchworth, UK, 1987.

9.  Toliyat, H. A. and N. A. Al-Nuaim, "Simulation and detection of dynamic air-gap eccentricity in salient-pole synchronous machines," *IEEE Trans. Industry Application*, Vol. 35, No. 1, 86–93, 1999.

10. Hsu, J. S. and J. Stein, "Effect of eccentricities on shaft signals studied through windingless rotors," *IEEE Trans. on Energy Conversion*, Vol. 9, No. 3, 564–571, 1994.

11. Hsu, J. S. and J. Stein, "Shaft signal of salient-pole synchronous machines for eccentricity and shorted-field-coil detections," *IEEE Trans. Energy Conversion*, Vol. 9, No. 3, 572–578, 1994.

12. Kim, C. E. and J. K. Sykulski, "Harmonic analysis of output voltage in synchronous generator using finite element method taking account of the movement," *IEEE Trans. Magnetics*, Vol. 38, No. 2, 1249–1252, Mar. 2002.

13. Faiz, J., B. M. Ebrahimi, B. Akin, and H. A. Toliyat, "Finite-element transient analysis of induction motors under mixed eccentricity fault," *IEEE Trans. Magnetics*, Vol. 44, No. 1, 66–74, Jan. 2008.

14. Bangura, J. F. and N. A. Demerdash, "Effects of broken bars/end-ring connectors and airgap eccentricities on ohmic and core losses of induction motors in asds using a coupled finite element-state space method," *IEEE Trans. Energy Conversion*, Vol. 15, No. 1, 40–47, Mar. 2000.

15. Thomson, W. T., "On line current monitoring and application of a finite element method to predict the level of static air gap eccentricity in three-phase induction motors," *IEEE Trans. Energy Conversion.*, Vol. 13, No. 14, 347–354, Dec. 1998.

16. Thomson, W. T. and A. Barbour, "An industrial case study of on-

line current monitoring and finite element analysis to diagnose air-gap eccentricity problems in large high voltage 3-phase induction motors," *Proc. 9th Int. Conf. Electr. Machines Drives*, No. 468, Conference Publication, 1999.

17. Faiz, J., I. Tabatabaei, and H. A. Toliyat, "An evaluation of inductances of a squirrel-cage induction motor under mixed eccentric conditions," *IEEE Trans. Energy Conversion*, Vol. 18, No. 2, 252–258, Jun. 2003.

18. Joksimovic, G. M., M. D. Durovic, J. Penman, and N. Arthur, "Dynamic simulation of dynamic eccentricity in induction machines — Finding function approach," *IEEE Trans. Energy Conversion*, Vol. 25, No. 2, 143–149, Jun. 2000.

19. Nandi, S., R. M. Bharadwaj, and H. A. Toliyat, "Performance analysis of a three-phase induction motor under mixed eccentricity condition," *IEEE Trans. Energy Conversion*, Vol. 17, No. 3, 392–399, Sep. 2002.

20. Nandi, S., S. Ahmed, and H. A. Toliyat, "Detection of rotor slot and other eccentricity related harmonics in a three phase induction motor with different rotor cages," *IEEE Trans. Energy Conversion*, Vol. 16, No. 3, 253–260, Sep. 2001.

21. Povinelli, R. J., J. F. Bangura, N. A. O. Demerdash, and R. H. Brown, "Diagnostics of bar and end-ring connector breakage faults in poly phase induction motors through a novel dual trackof time-series data mining and time-stepping coupled FE-state space modeling," *IEEE Trans. Energy Conversion,* Vol. 17, No. 1, 39–46, 2002.

22. Cundev, D. and L. Petkovska, "Computation of electromechanical characteristics of salient poles synchronous motor with damper based on FEM," *Journal of Materials Processing Technology*, Vol. 161, 241–246, 2005.

23. Faiz, J., B. M. Ebrahimi, and M. B. B. Sharifian, "Time stepping nite element analysis of broken bars fault in a three-phase squirrel-cage induction motor," *Progress In Electromagnetics Research*, PIER 68, 53–70, 2007.

24. Faiz, J. and B. M. Ebrahimi, "Mixed fault diagnosis in three-phase squirrel-cage induction motor using analysis of air-gap magnetic field," *Progress In Electromagnetics Research*, PIER 64, 239–255, 2006.

25. Tu, X., L. A. Dessaint, M. E. Kahel, and A. O. Barry, "A new model of synchronous machine internal faults based on winding distribution," *IEEE Trans. Industrial Electronics*, Vol. 53, No. 6, 1818–1828, Dec. 2006.

26. Reichmeider, P. P., C. A. Gross, D. Querrey, D. Novosel, and S. Salon, "Internal faults in synchronous machines Part I: The machine model," *IEEE Trans. Energy Conversion*, Vol. 15, No. 4, 376–379, Dec. 2000.

27. Faiz, J., B. M. Ebrahimi, M. Valavi, and H. A. Toliyat, "Mixed eccentricity fault diagnosis in salient-pole synchronous generator using modified winding function method," *Progress In Electromagnetics Research B*, Vol. 11, 155–172, 2009.